Acta Astronautica 170 (2020) 499–508

Contents lists available at ScienceDirect

Acta Astronautica

journal homepage: www.elsevier.com/locate/actaastro

Research paper

Using multilayer polymer PI/Pb composites for protection against X-ray bremsstrahlung in outer space

N.I. Cherkashina[a,*], V.I. Pavlenko[a], A.V. Noskov[b], N.I. Novosadov[a], E.S. Samoilova[a]

[a] Institute of Chemical Technology, Radiation Monitoring Laboratory, Belgorod State Technological University Named After V.G. Shoukhov, Belgorod, 308012, Kostyukov Str., 46, Russia

[b] Belgorod State National Research University, Pobedy str., 85, Belgorod, 308015, Russia

ARTICLE INFO

Keywords:
Multilayer composite
Track membranes
Template synthesis
Nanodispersed lead
X-ray bremsstrahlung

ABSTRACT

This paper presents data about the radiation-protective characteristics of multilayer polyimide/lead (PI/Pb) composites for X-ray radiation. Multilayer composites were obtained by collecting lead-filled polyimide track membranes into a sandwich of the required thickness. (^{241}Am) (E = 59.5 keV) and (^{109}Cd) (E = 88 keV) isotopes were used as an X-ray radiation source. To assess the effect of lead filler particle size on the radiation-protective characteristics of a multilayer structure, data are presented on mathematically modeling the passage of 10–88 keV wavelength X-rays with through a composite. The experimental values of the attenuation coefficients of X-ray waves for a multilayer structure are 12–15% higher than the calculated ones. The increase in the attenuation coefficients obtained experimentally, compared with theoretical, is explained by using the proposed multilayer structure with lead particles in the nanoscale range.

1. Introduction

A long spacecraft (SC) flight is accompanied by a significant increase in the accumulated dose of ionizing radiation, which is detrimental to crew members. At ISS altitude, there are serious radiation safety concerns. First, in the area of the South Atlantic, there is the so-called Brazilian, or South Atlantic, magnetic anomaly. Here, the Earth's magnetic field is unusually weak, and with it, the lower radiation belt appears closer to the surface. Second, the cosmonaut in space is threatened by galactic radiation – a stream of charged particles from all directions and at great speed – generated by supernova explosions or the activity of pulsars, quasars, and other anomalous stellar bodies [1,2].

Primary cosmic rays consist mainly of protons (90%); α-particles (7%); other atomic nuclei, up to the heaviest; and a small number of electrons, positrons, and photons of higher energy [3,4]. The greatest danger to the hull and elements of spacecraft located on its outer side are the protons of the Earth's radiation belts, with an energy of 1–30 MeV, and electrons, with an energy of 1–5 MeV [5]. For the year of flight at the ISS, the cosmonaut receives a dose of approximately 200 mSv/year [6]. For cosmonauts, the inner radiation belt protons provide the highest consistent hourly dose, while the relativistic electrons and/or bremsstrahlung in the outer radiation belt and solar energetic particles provide the most extreme hourly doses [7]. The bremsstrahlung an energy of 10–100 keV is formed resulting from relativistic electrons interaction with the hull and various elements of the spacecraft [8,9]. Auroral X-ray bremsstrahlung has been observed from balloons and rockets since the 1960s and from spacecraft since the 1970s [10].

The bremsstrahlung radiation can greatly harm the health of astronauts [11]. It is known that in SC orbits, where there are high fluxes of energetic electrons, the absorbed radiation dose inside the SC is not mainly determined by electrons, but by their Bremsstrahlung [12]. Fig. 1 shows that in a geostationary orbit, the absorbed dose of radiation from hard electromagnetic radiation under the radiation protection of 11 mm aluminum is more than two thousand times higher than the dose of radiation from electrons that generate this radiation [13]. The data presented in Fig. 1 are given for the situation when an aluminum screen is modifying the incoming radiation and the radiation is absorbed by human tissue inside the screen. Therefore, using substances with a large atomic number is avoided for structural materials in SC and, most often, aluminum and its alloys are used [14–17]. X-ray bremsstrahlung generated by the interaction of fast electrons with the aluminum body of the SC causes potential damage to the health of the crew inside the SC. The most vulnerable places on the ISS are the cosmonaut cabins, where they rest. There is no additional mass, they

Abbreviations: PI, polyimide; ISS, International Space Station; SC, spacecraft

* Corresponding author.
E-mail addresses: cherkashina.ni@bstu.ru (N.I. Cherkashina), natalipv13@mail.ru (V.I. Pavlenko).

https://doi.org/10.1016/j.actaastro.2020.02.022
Received 4 October 2019; Received in revised form 6 January 2020; Accepted 10 February 2020
Available online 15 February 2020

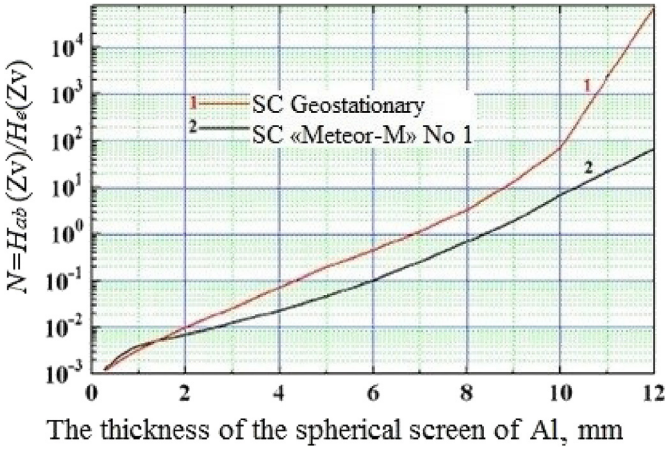

Fig. 1. The ratio of equivalent dose (H_{ab}) from hard electromagnetic radiation to the equivalent dose from relativistic electrons (H_e) in the orbits of a geostationary satellite and SC "Meteor-M" No 1 under a screen of various thicknesses of Al.

are there without protective suits and only a metal wall several millimeters thick separates cosmonauts from outer space.

There has recently been active development to create additional local radiation protection for cosmonauts inside SC, including the use of vests [18–21]. Using pure metals to protect against X-ray bremsstrahlung inside the SC will significantly increase the payload mass, which will lead to increased fuel consumption and an increase in the cost of the space mission as a whole. In addition, pure metal does not have the necessary flexibility to create radiation-protective vests for cosmonauts.

Many studies in the field of protection against x-ray and gamma radiation are devoted to developing polymer composites containing metal or metal oxides as a filler [22–27]. Using fillers in the form of nanosized particles significantly increases the radiation protective characteristics of such composites in comparison to using coarse particles for the same wt% fillers [28–30]. The introduction nano-scaled fillers into polymer matrices is more efficient in attenuating radiation since nanomaterials are more uniform and have less agglomeration in the composite and therefore can enhance the shielding ability of material [31,32].

Gulbin et al. established that using tungsten and lead oxide nanocrystalline powders for radiation-protective materials allow a 1.34–1.43 times increased radiation protection efficiency compared to analog material with coarse crystals [33]. El-Khatib et al. studied the effect of particle size and weight percentage of CdO micro-sized and nano-sized particles on the gamma radiation shielding ability of CdO/HDPE. The experimental results reveal that, the composites filled with nano-CdO have better γ-radiation shielding ability compared to that filled with micro-CdO at the same weight fraction. A relative increase rate of about 16% is obtained with nano-CdO content of 40 wt% at 59.53 keV [32].

Mesbahi et al. showed applying nanoparticles in radiation-absorbing materials (PbO_2, Fe_2O_3, WO_3, and H_4B) leads to better neutron absorption and dispersion of Roentgen- and gamma radiation. The materials doped with nano-sized particles showed a higher neutron removal cross-section (7%) and photon attenuation coefficient (8%) relative to micro-particles [34].

This work is devoted to studying the radiation protective characteristics of multilayer polymer composites for X-ray radiation as one of the negative factors of outer space. Composites were prepared by bonding several layers of polyimide track membranes filled with nanosized metallic lead. Polymer track membranes are the thin polymer films (10–25 μm) with many through holes at the nanoscale. For their synthesis, polymer films are irradiated with a stream of high-energy heavy ions [35–37]. Each ion along its path damages polymer

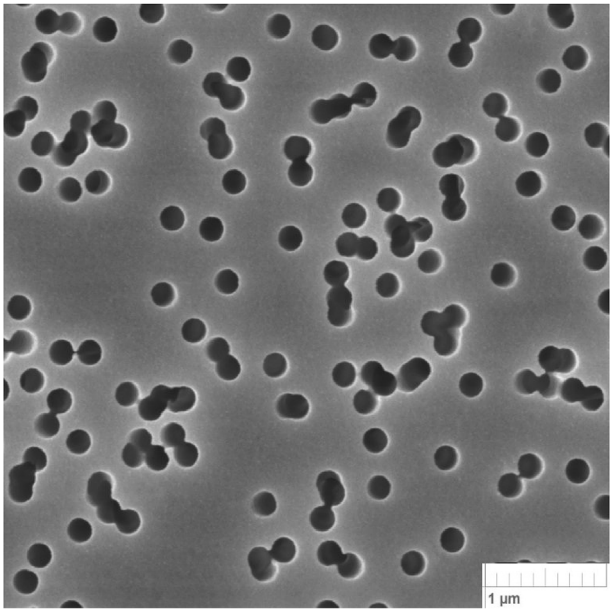

a

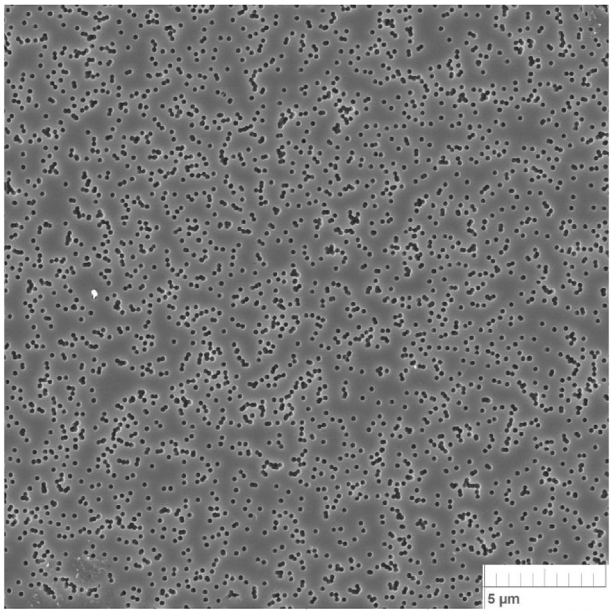

b

Fig. 2. SEM images of the surface of the polyimide track membrane.

molecules, leaving a trace known as a track (hence the name of "track" membrane).

The mass attenuation and absorption coefficients of X-ray waves for multilayer composites at various energies were studied experimentally and theoretically.

2. Methodology

2.1. PI/nanodispersed Pb composite synthesis

To obtain flexible polymer multilayer composites, polyimide track (nuclear) membranes manufactured by Ion Track Technology for Innovative Products (it4ip), Belgium, were used as a matrix. The track membrane was a thin polyimide film (25 μm thick) with many through holes, a 200 nm diameter, and $5{\cdot}10^8$ cm^{-1} pore density. A micrograph of

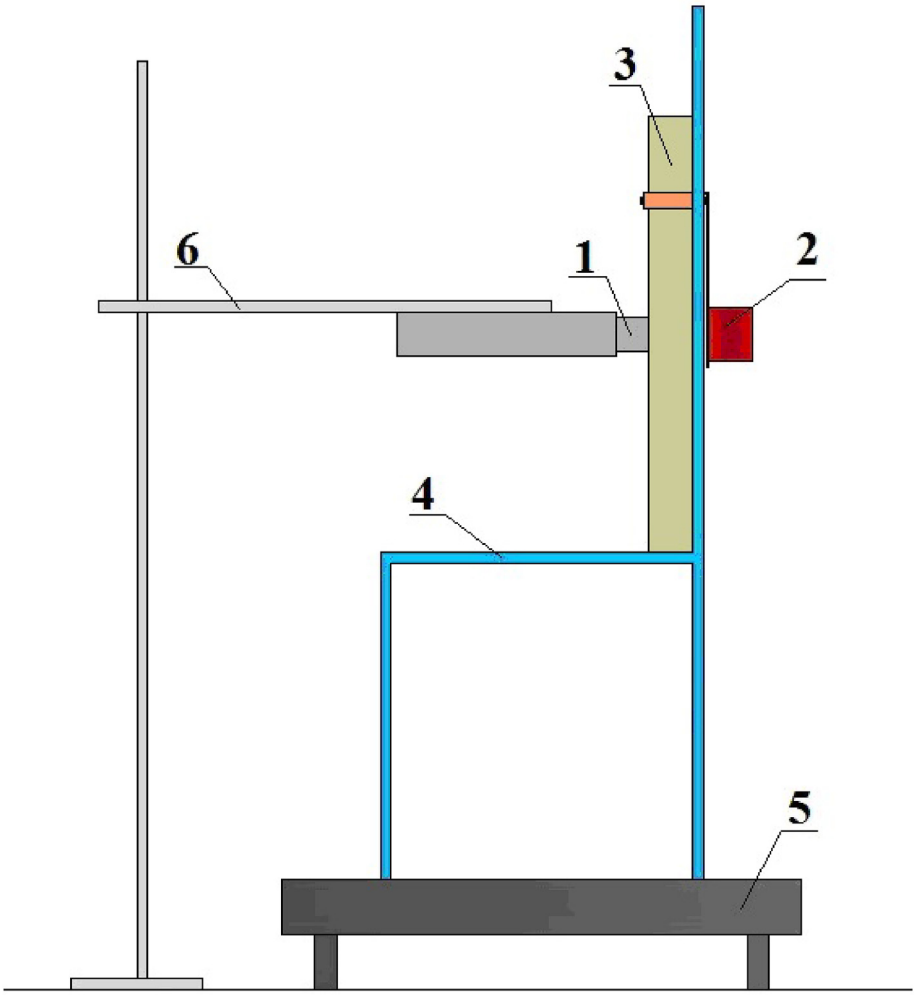

Fig. 3. The scheme for measuring the attenuation coefficient of the photon beam when passing through the studied composites: 1 – Dosimeter of X-ray radiation DKR-AT1103 M; 2 – X-ray source; 3 – The investigated composite; 4 – Specialized rack; 5 – Platform; 6 – Tripod.

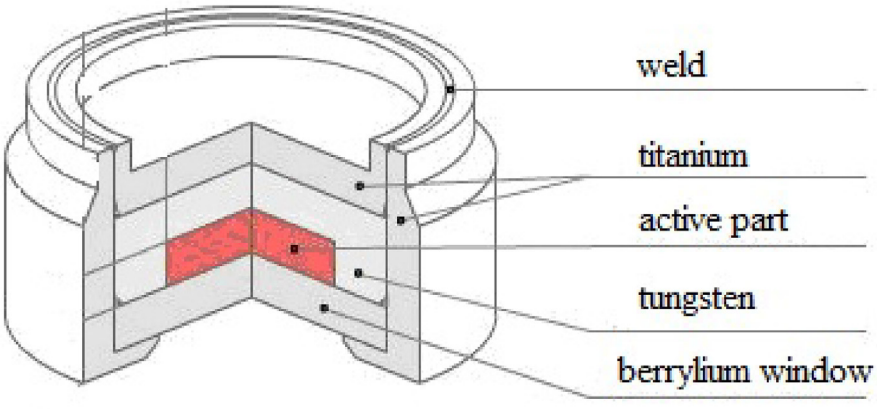

Fig. 4. The layout of the X-ray source in the ceramic matrix.

the surface of the polyimide track membrane is shown in Fig. 2.

The introduction of a filler–nanodispersed metallic lead–was carried out by the template synthesis method. This method is widely used to fill the pores of track membranes with various metals and is well described in Refs. [38–43]. The essence of this method is galvanic metal deposition from a solution of its salt into the etched through channels (pores) of the track membrane. A lead-based metal coating deposited on one side of a polyimide track membrane was used as a cathode for depositing nanodispersed lead. The cathode was deposited by method dual magnetron sputtering in a UniCoad 200 vacuum unit with an unbalanced magnetic system. The coating thickness was 50 nm.

The electrolyte composition was lead tetrafluoroborate $Pb(BF_4)_2$ – 200 g/l, hydrofluoric acid HBF_4 – 45 g/l, and wood glue – 1 g/l.

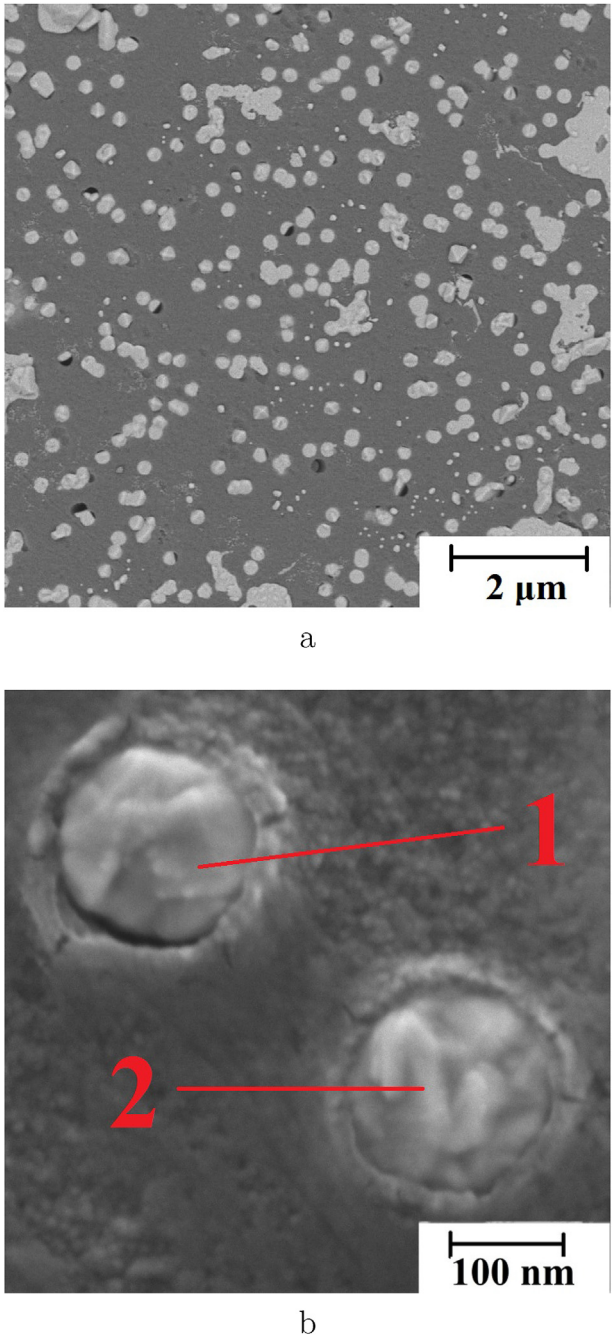

Fig. 5. SEM images of a surface of the track membrane after galvanic deposition of lead.

The galvanic process was carried out at room temperature using an IPC-Pro 3A potentiostat-galvanostat. The electrodeposition mode was used at a 400 mV fixed potential for 27 min.

Forming the multilayer structure of the composite was carried out by collecting lead-filled membranes into a sandwich of the required thickness. Polyamic acid was used (manufactured by the Institute of Plastics named after Petrov JSC, Russia) for bonding the filled membranes with each other. Lead-filled polyimide track membranes with a layer of polyamic acid, assembled into a sandwich of the required thickness, were placed in a steel mold and subjected to hot pressing at 250–270 °C and 200 MPa for 30 min.

2.2. Research methods

The crystal structure of nanodispersed lead was investigated using X-ray diffraction (ARL X'TRA, ThermoTechno) with a CuKα source in the 2θ 30 – 100° angle range in asymmetric coplanar mode with a sliding angle of incidence $\alpha = 3°$ (θ-scan) to eliminate peaks from the substrate. Phase identification and peak indexing were performed using JCPDF [44].

The surface morphologies were examined using a scanning electron microscope (TESCAN MIRA 3 LMU).

Studies to assess the radiation-protective characteristics of composites for X-ray radiation were carried out at the Center for Radiation Monitoring, Belgorod State Technological University named after V. G. Shukhov. A diagram of an experimental bench designed to determine the attenuation coefficient of a photon beam passing through the studied composites is shown in Fig. 3.

In the experiment, the differential and integral energy distributions of the flux densities of the gamma rays in the incident radiation were measured, from the source without radiation protective material and behind the materials under study.

The studied composite was placed in a specialized rack placed on the platform. The radiation source was installed in a "glass" in the center of the material, as close as possible to the end surface of the material. (^{241}Am) (half-life $T_{1/2}$, 432.1 years; energy of the emitted photons, E = 59.5 keV; activity of the radioisotope, 4.6 μCi and (^{109}Cd) (half-life $T_{1/2}$, 461.4 years; energy of the emitted photons, E = 88 keV; activity of the radioisotope, 15 μCi) isotopes were used as an X-ray source. The (^{241}Am) and (^{109}Cd) radionuclides were distributed inside a ceramic matrix placed in a tungsten alloy insert (Fig. 4). The insert with the matrix was placed in a monel metal capsule with a beryllium window, welded using laser welding (Fig. 4). The DKR-AT1103 M X-ray dosimeter was mounted on a tripod and fit snugly against the surface of the material (Fig. 3). The distance from the source to the detector was 200 mm.

The transmitted radiation intensity was counted for 25 min for each sample. All measurements were repeated five times at the same experimental conditions.

3. Results and discussion

3.1. Properties of the PI/nanodispersed Pb composites

The microstructure of the track membrane surface after galvanic lead deposition is shown in Fig. 5. Analysis of the obtained SEM image shows that during electrodeposition, the pores of the track membrane are completely filled. An electron probe microanalysis of the synthesized substance in the pores of the membrane was carried out. The spectra of the energy-dispersive microanalysis of the track membrane and filled pores are shown in Fig. 6. According to the obtained atomic composition data, Pb atoms are concentrated at points 1 and 2 (Fig. 6b) (the depth of electronic scanning in the material at 7 kV does not exceed 0.05 μm). The presence of other atoms of the elements was not fixed.

To perform an X-ray structural analysis of the compound obtained in the pores of the track membrane, the polyimide layer was etched in a 25% solution of ammonia water, NH_4OH at room temperature for 4 h. After removing the polyimide matrix (Fig. 7), the peaks at 2θ angles of 31.44°, and 108.92°, characteristic of (111), (222), and (333) lead planes, respectively [45], are distinctly observed in the X-ray diffraction spectra. The value of the constant face-centered cubic cell $a = 4.950$ Å nm is in full agreement with the reference data, $a = 4.959$ Å (PDF card No. 4–686); the average size of lead crystallites was 25 ± 1 nm.

Table 1 presents the physicomechanical test results for a multilayer composite obtained by collecting lead-filled membranes into a 2.4 mm thick sandwich. Analysis of the data obtained in Table 1 indicates the high strength characteristics of the obtained composite (tensile strength

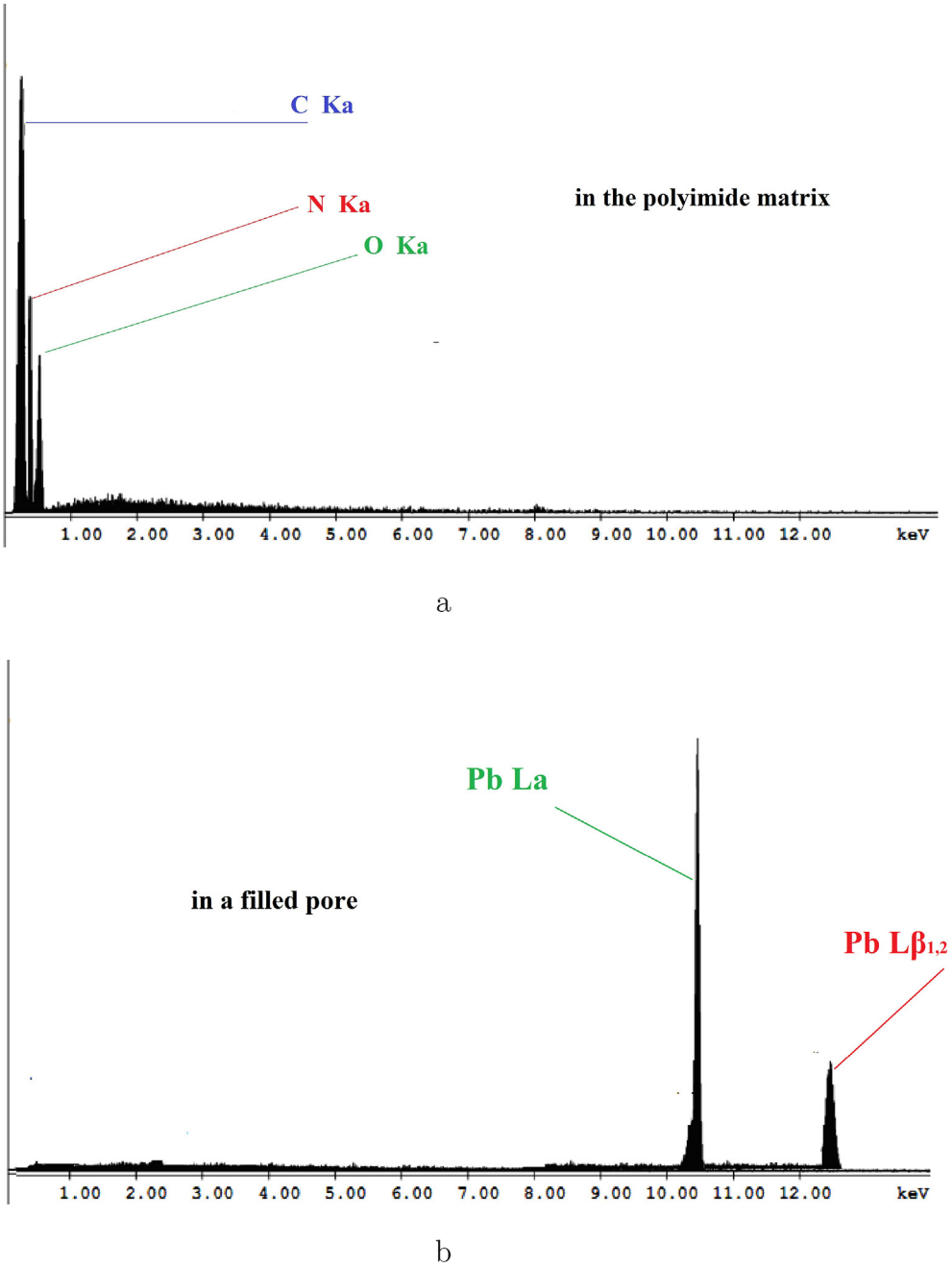

Fig. 6. Spectrum of energy dispersive microanalysis of a polyimide track membrane (a) and in a filled pore (b).

108 MPa, tensile modulus 2250 MPa). Polyimide without filler is an insulator with a large volume resistivity (>10^{14}Ω m). The introduction of lead into the pores of polyimide membranes leads to a significant decrease in volume resistivity (10^3 Ω m), which indicates the metallic conductivity (high resistance through the 50 nm lead film).

3.2. Theoretical calculations of the interaction of X-rays with PI/Pb composite

To assess the influence of lead filler particle size on the radiation-protective characteristics of the multilayer structure, mathematically modeling the passage of 10–88 keV wavelength X-rays through the composite was carried out. In the simulation, the influence of the filler particle size was not included; only the percentage of atoms of each element included in the PI/Pb composite was included. Material design consisted of N layers (N_{max} = 80). The thickness of each layer corresponds to the thickness of a 25 μm polyimide membrane. The films are tightly pressed against each other. Between each film, there is a 50 nm thick lead sheet (the thickness corresponds to the thickness of the lead cathode coating). The target thickness formula is T = N·25μm + (N−1)·50 nm. At N_{max} = 80, the target thickness was T = 2.4 mm. The density of the multilayer structure with lead was 4.21 g/cm^3. The lead content is 76.14% (by weight). The chemical elemental atomic composition of the multilayer structure is presented in Table 2.

The mass attenuation and absorption coefficients of X-ray waves for multilayer composites at various energies were studied experimentally and theoretically. Linear attenuation coefficient is a constant that describes the fraction of attenuated incident photons in a monoenergetic beam per unit thickness of a material. The absorption coefficient is a constant that describes the fraction of absorbed incident photons in a monoenergetic beam per unit thickness of a material [46].

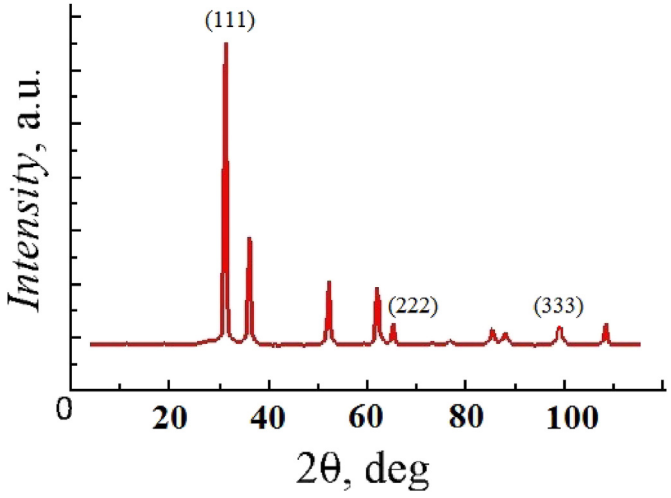

Fig. 7. X-ray diffractograms of electrodeposited matter in the pores.

Table 1
Physico-mechanical and electrical characteristics of the multilayer composite.

No	Name of characteristics	Indicators
1	Tensile strength, MPa	108
2	Elongation in tension, %	9.5
3	Tensile modulus, MPa	2250
4	Volume resistivity, Ω·m	10^3
5	Heat conductivity coefficient, W/m·K	11.2
6	Specific heat capacity from 20 to 300 °C, J/kg·K	$2.7{\cdot}10^3$
7	The coefficient of linear thermal expansion (20 − 250)°C, K^{-1}	$32{\cdot}10^6$

Table 2
Chemical atomic elemental composition of a multilayer structure.

Atom content, wt%				
C	N	O	H	Pb
16.25	1.81	5.16	0.64	76.14

The attenuation coefficient of photon radiation includes the interaction coefficients due to the photoelectric effect, incoherent scattering by coupled electrons (Compton scattering), and the formation of electron-positron pairs. For the photon energies under consideration from 10 to 88 keV, this is mainly a photoelectric effect. The absorption coefficient also includes the interaction coefficients due to absorption by the photoelectric effect, absorption by incoherent scattering by bound electrons, and absorption during the formation of electron-positron pairs. At the photon energies under consideration, this is mainly absorption by the photoelectric effect. The remaining effects were not included in the calculations.

The expression describing the cross-sections of the process of the photoelectric effect on an atom has the following form:

$$\sigma_{fot} = 4\pi r_e^2 \alpha^4 Z^5 G_f(E),$$
$$G_f(E) = \frac{(2+\varepsilon)^{3/2}}{\varepsilon^{7/2}}\left(\frac{4}{3} + (1+\varepsilon)\frac{\varepsilon-1}{\varepsilon+2}\left(1 - \frac{1}{2(\varepsilon+1)\sqrt{\varepsilon(2+\varepsilon)}}\right)\right.$$
$$\left. \times \times \ln\left(\frac{1+\varepsilon+\sqrt{\varepsilon(2+\varepsilon)}}{1+\varepsilon-\sqrt{\varepsilon(2+\varepsilon)}}\right)\right), \quad (1)$$

where $\varepsilon = E/m_e{\cdot}c^2$, E is the x-ray energy, $m_e{\cdot}c^2 = 0.511$, MeV is the rest energy of an electron, $r_e = e^2/m_e{\cdot}c^2 = 2.8{\cdot}10^{-13}$ cm — the classical electron radius, and $\alpha = 1/137$ — the fine structure constant.

Since the multilayer structure under study consists of atoms of several elements (C, N, O, H, Pb), the Bragg Rule (Bragg's composition law) was used in the calculations:

$$S = -(1/\rho)dE/dx = (1/M)\sum_{n_i} A_i[-(1/\rho)dE/dx]_i, \quad (2)$$

where S is the inhibitory ability of the composite, M is the molecular weight of the compound, and n_i is the number of atoms of the ith grade with atomic mass A_i per unit volume.

Then, the attenuation coefficient of the X-ray flux due to the photoelectric effect has the form:

$$\mu_f = 4\pi r_e^2 \alpha^4 N_\alpha \left(\rho_C \frac{Z_C^5}{A_C} + \rho_N \frac{Z_N^5}{A_N} + \rho_0 \frac{Z_O^5}{A_O} + \rho_H \frac{Z_H^5}{A_H} + \rho_{Pb} \frac{Z_{Pb}^5}{A_{Pb}}\right) G_f(E) \quad (3)$$

where ρ_i is the density of the corresponding element, Z_i is the serial number of the corresponding element, A_i is the atomic mass of the corresponding element, and N_A is Avogadro's number ($6.02{\cdot}10^{23}$).

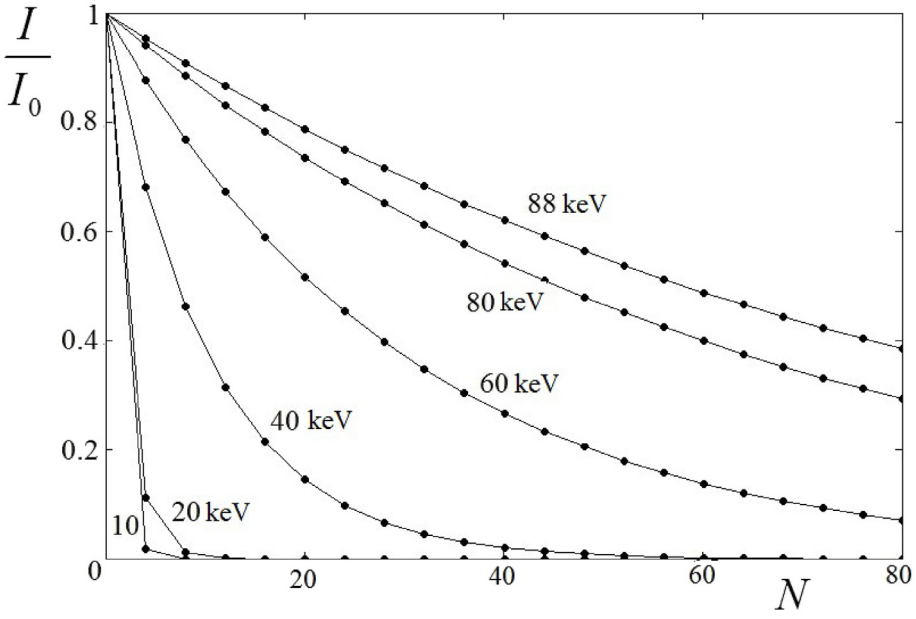

Fig. 8. The change in the intensity of a photon beam of various energies due to absorption, depending on the number of layers N of the multilayer structure.

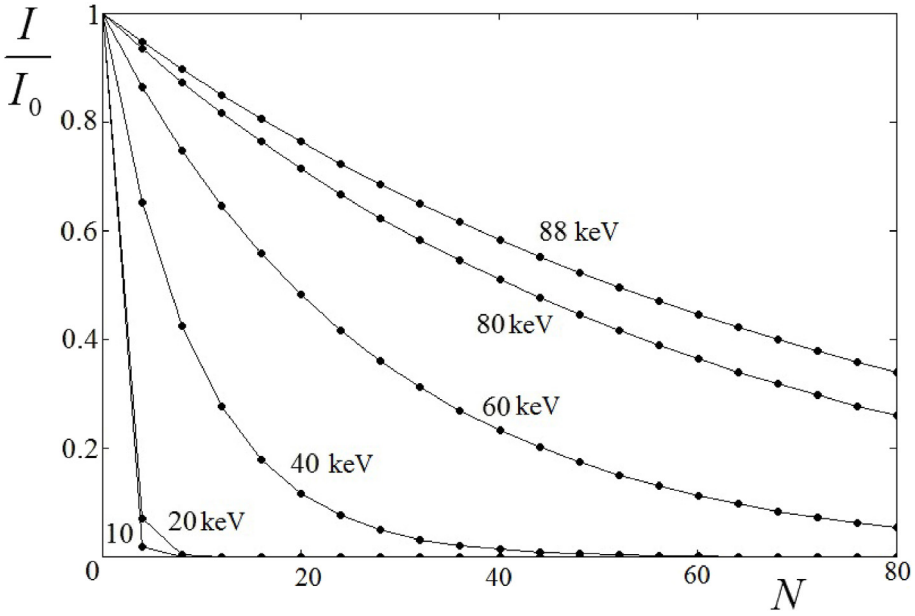

Fig. 9. The change in the intensity of the photon beam of various energies due to attenuation depending on the number of layers N of the multilayer structure.

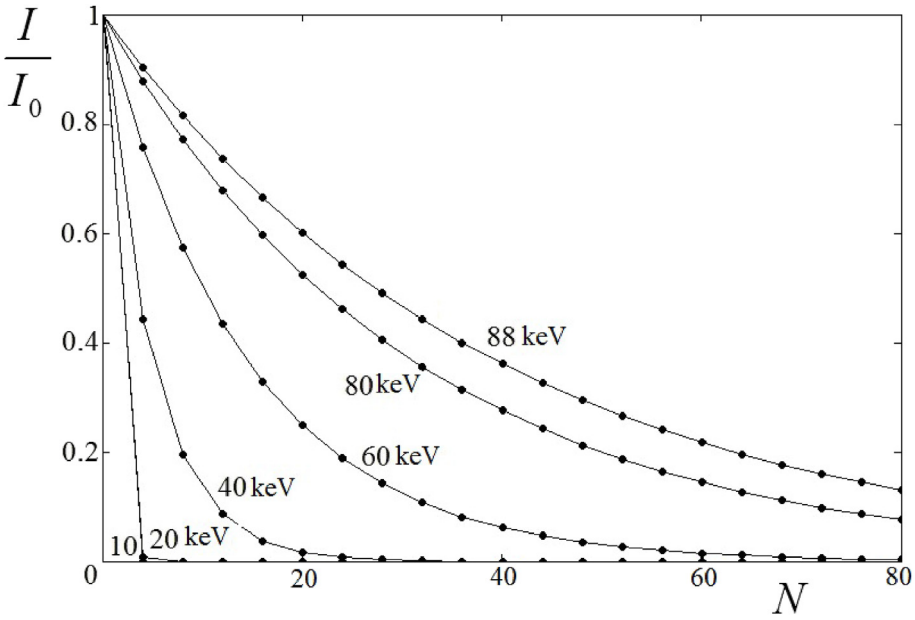

Fig. 10. The change in the intensity of the photon beam of various energies due to absorption and attenuation depending on the number of layers N of the multilayer structure.

Table 3
The calculated values of the mass attenuation and absorption coefficients of X-ray waves for a multilayer structure (N_{max} = 80) and lead.

E, keV	Mass attenuation coefficient, μ_{at} = (cm^2/g)		Mass absorption coefficients, μ_{ab}(cm^2/g)		$\mu_{at} + \mu_{ab}$(cm^2/g)	
	Multilayer structure	Lead	Multilayer structure	Lead	Multilayer structure	Lead
10	94.35	123	94.32	123	188.68	246
20	63.15	82.8	55.04	68.3	115.19	151.1
40	10.17	13.3	9.15	12	19.33	25.3
60	3.45	4.48	3.13	4.10	6.58	8.58
80	1.59	2.05	1.45	1.9	3.05	3.95
88	1.32	1.63	1.25	1.48	2.57	3.11

Figs. 8–10 show the calculated data on the change in intensity of a photon beam of various energies due to absorption (Fig. 8), due to attenuation (Fig. 9), and due to absorption and attenuation (Fig. 10) depending on the number of layers, N, of a multilayer PI/Pb structure. From the obtained data, the values of attenuation and absorption coefficients are close for all studied samples and X-ray energies, while the attenuation coefficients are not much larger than the absorption coefficients. The effects of X-ray absorption in the studied energy range (up to 88 keV) in lead are mainly due to the photoelectric effect. And the scattering effects are due to the Compton effect. For the X-ray energies under study, the contribution of the photoelectric effect and the Compton effect is practically the same [47].

As the X-ray energy increases from 10 to 88 keV, the intensity of the transmitted photon beam decreases markedly. A similar situation occurs with an increase in the number of layers.

Table 4
X-ray attenuation coefficients for a multilayer structure obtained by calculation and experimental method.

Parameter	X-ray energy			
	E = 59.5 keV (^{241}Am)		E = 88 keV(^{109}Cd)	
	Calculated value	Experimental value	Calculated value	Experimental value
Linear attenuation coefficient μ, cm $^{-1}$	14.10	15.79 ± 1.23	5.56	6.39 ± 0.49
Mass attenuation coefficient μ_{at}, cm^2/g	3.35	3.75 ± 0.29	1.32	1.52 ± 0.17

Table 3 presents the calculated mass attenuation and absorption coefficients of X-ray waves for a multilayer structure at different wave and lead energies for comparison.

A comparison of the calculated mass attenuation and absorption coefficients of X-ray waves for the multilayer structure and pure lead shows that the calculated coefficients of the proposed composite structure are 22–24% lower than the values of pure lead (Table 3). If we compare the density of the multilayer structure (4.21 g/cm^3) and lead (11.3 g/cm^3), then the density of the metal will be 2.6 times higher than the density of the proposed composite structure. Thus, for using radiation-protective material, the developed composite structure has improved overall mass characteristics compared to pure lead.

3.3. Experimental results of X-ray interaction with PI/Pb composite

The linear attenuation coefficients (μ) of X-ray can be extracted by the standard equation:

$$N = N_0 \cdot e^{-\mu d} \quad (4)$$

where N — the measured count rates in detector with the thickness absorber, d (cm); N_0 — the measured count rates in detector without the thickness absorber.

The mass attenuation coefficients of X-ray was found as a ratio of the linear gamma photon attenuation coefficient μ to material density ρ:

$$\mu_m = \frac{\mu}{\rho} \quad (5)$$

Table 4 presents the experimental data on the linear and mass attenuation coefficients of X-ray waves for a multilayer structure (N_{max} = 80) at E = 59.5 keV (^{241}Am) and E = 88 keV (^{109}Cd).

An analysis of the data in Table 4 shows that for the energies under consideration, the experimental values of the attenuation coefficients of X-ray waves for a multilayer structure are 12–15% higher than the calculated ones. The 12–15% significantly larger than the error of the devices in the experiment. The measurement error (5–7%) is by errors in the detector during pulse counting, as well as errors in measuring the thickness of the sample.

The increase in the attenuation coefficients obtained experimentally, compared with theoretical, can be explained by the use of the proposed multilayer structure in which lead is present in the nanoscale range. Nanosized particles are known to significantly increase the radiation resistance of the material to gamma, X-ray, and neutron radiation compared with micro-sized particles [28–30]. The introduction nano-scaled fillers into polymer matrices is more efficient in attenuating radiation since nanomaterials are more uniform and have less agglomeration in the composite and therefore can enhance the shielding ability of material [31,32]. Since the simulation did not take into account the influence of the filler particle size, using nanodispersed lead, in the authors' opinion, led to an increase in the attenuation coefficients of X-ray radiation in this work.

4. Conclusions

The possibility of obtaining a multilayer polymer structure by "bonding" several layers of polyimide track membranes filled with nanodispersed metallic lead was established. High radiation protective characteristics are shown for X-ray radiation in synthesized multilayer polymer composites. For the considered X-ray energies (10–88 keV), the experimental attenuation coefficients of the X-ray waves for the multilayer structure are 12–15% higher than the calculated ones. The 12–15% difference is much larger than the error of the devices in the experiment, which proves that the use of the proposed multilayer structure, in which lead particles are present in the nanoscale range, increases the attenuation coefficients of x-ray radiation compared with the use of coarse particles. The results can be used to create promising radiation-protective shields and vests for cosmonaut protection during long space missions. Further research will be aimed at studying the radiation-protective characteristics of the proposed from charged particles of the cosmic spectrum.

Funding

The work was supported by a project of the Russian Science Foundation (19–79 – 10064).

References

[1] J. Barthel, N. Sarigul – Klijn, Radiation production and absorption in human spacecraft shielding systems under high charge and energy Galactic Cosmic Rays: material medium, shielding depth, and byproduct aspects, Acta Astronaut. 144 (2018) 254–262, https://doi.org/10.1016/j.actaastro.2017.12.040.
[2] M.H.Y. Kim, G. De Angelis, F.A. Cucinotta, Probabilistic assessment of radiation risk for astronauts in space missions, Acta Astronaut. 68 (2011) 747–759, https://doi.org/10.1016/j.actaastro.2010.08.035.
[3] C. Amsler, K.A. Olive, K. Agashe, Review of cosmic rays, Phys. Lett. B 667 (2008) 1–1340 2008.
[4] A. Annila, Cosmic rays report from the structure of space, Adv. Astronomy (2015), https://doi.org/10.1155/2015/135025 2015, Article ID 135025.
[5] A.S. Kovtyukh, Ion composition of the Earth's radiation belts in the range from 100 keV to 100 MeV/nucleon100 MeV/nucleon: fifty years of research, Space Sci. Rev. 214 (2018) 124–153, https://doi.org/10.1007/s11214-018-0560-z.
[6] M. Durante, F.A. Cucinotta, Physical basis of radiation protection in space travel, Rev. Mod. Phys. 83 (2011) 1245–1281, https://doi.org/10.1103/RevModPhys.83.1245.
[7] T.P. Dachev, N.G. Bankov, B.T. Tomov, Yu.N. Matviichuk, Pl.G. Dimitrov, D.P. Häder, G. Horneck, Overview of the ISS radiation environment observed during the ESA EXPOSE-R2 mission in 2014 – 2016, Space Weather 15 (2017) 1475–1489, https://doi.org/10.1002/2016SW001580.
[8] W. Xu, R.A. Marshall, X. Fang, E. Turunen, A. Kero, On the effects of bremsstrahlung radiation during energetic electron precipitation, Geophys. Res. Lett. 45 (2018) 1167–1176, https://doi.org/10.1002/2017GL076510.
[9] W. Xu, R.A. Marshall, Characteristics of energetic electron precipitation estimated from simulated bremsstrahlung X–ray distributions, JGR Space Phys. 124 (2019) 2831–2843, https://doi.org/10.1029/2018JA026273.
[10] A. Bhardwaj, C.M. Lisse, X-rays in the solar system, Chapter 35 in Encyclopedia of the Solar System, second ed., Elsevier Inc., 2007, pp. 637–658.
[11] B.M. Rabin, An evaluation of the relative behavioral toxicity of heavy particles, Biological Effects and Physics of Solar and Galactic Cosmic Radiation Part A, Springer US, 1993, pp. 227–233, , https://doi.org/10.1007/978-1-4615-2918-7.
[12] M.O. Riazantseva, I.N. Myagkova, M.V. Karavaev, E.E. Antonova, I.L. Ovchinnikov, B.V. Marjin, M.A. Saveliev, V.M. Feigin, M.V. Stepanova, Enhanced energetic electron fluxes at the region of the auroral oval during quiet geomagnetic conditions November 2009, Adv. Space Res. 50 (2012) 623–631, https://doi.org/10.1016/j.asr.2012.05.015.
[13] I.P. Bezrodnykh, Y.I. Morozova, A.A. Petrukovich, S.G. Kazantsev, I.V. Kochetov, V.T. Semenov, Brake radiation of electrons in the substance of the space vehicle. Calculation method, Questions of electromechanics, Works VNIIEM 120 (2011) 37–44 (In Russian).
[14] E.V. Shirshneva – Vaschenko, P.S. Shirshnev, Zh.G. Snezhnaia, L.A. Sokura,

V.E. Bougrov, A.E. Romanov, Zinc oxide aluminum doped slabs for heat-eliminating coatings of spacecrafts, Acta Astronaut. 163 (2019) 107–111, https://doi.org/10.1016/j.actaastro.2019.07.005.
[15] W. Xuezhong, H. Jie, K. Fawei, J. Lin, L. Jin, S. Qiang, L. Sen, Preliminary study on shielding performance of debris shield with the rear wall combining light materials and an aluminum plate, Int. J. Impact Eng. 124 (2019) 31–36, https://doi.org/10.1016/j.ijimpeng.2018.10.006.
[16] P. Zhang, Z. Gong, D. Tian, G. Song, Q. Wu, Y. Cao, K. Xu, M. Li, Comparison of shielding performance of Al/Mg impedance-graded-material-enhanced and aluminum Whipple shields, Int. J. Impact Eng. 126 (2019) 101–108, https://doi.org/10.1016/j.ijimpeng.2018.12.007.
[17] J. Barthel, N. Sarigul – Klijn, Radiation production and absorption in human spacecraft shielding systems under high charge and energy Galactic Cosmic Rays: material medium, shielding depth, and byproduct aspects, Acta Astronaut. 144 (2018) 254–262, https://doi.org/10.1016/j.actaastro.2017.12.040.
[18] P. Spillantini, Active shielding for long duration interplanetary manned missions, Adv. Space Res. 45 (2010) 900–916, https://doi.org/10.1016/j.asr.2010.01.025.
[19] I.S. Peracchi, J. Vohradsky, S. Guatelli, D. Bolst, L.T. Tran, D.A. Prokopovich, A.B. Rosenfeld, Modelling of the Silicon-On-Insulator microdosimeter response within the International Space Station for astronauts' radiation protection, Radiat. Meas. 128 (2019) 106182, https://doi.org/10.1016/j.radmeas.2019.106182.
[20] U. Straube, T. Berger, G. Reitz, R. Facius, C. Fuglesang, T. Reiter, V. Damann, M. Tognini, Operational radiation protection for astronauts and cosmonauts and correlated activities of ESA Medical Operations, Acta Astronaut. 66 (2010) 963–973, https://doi.org/10.1016/j.actaastro.2009.10.004.
[21] M. Mirzaei, M. Zarrebini, A. Shirani, M. Shanbeh, S. Borhani, X-ray shielding behavior of garment woven with melt-spun polypropylene monofilament, Powder Technol. 345 (2019) 15–25, https://doi.org/10.1016/j.powtec.2018.12.069.
[22] A.K. Singh, R.K. Singh, B. Sharma, A.K. Tyagi, Characterization and biocompatibility studies of lead free X-ray shielding polymer composite for healthcare application, Radiat. Phys. Chem. 138 (2017) 9–15, https://doi.org/10.1016/j.radphyschem.2017.04.016.
[23] R. Li, Y. Gu, G. Zhang, Z. Yang, M. Li, Z. Zhang, Radiation shielding property of structural polymer composite: continuous basalt fiber reinforced epoxy matrix composite containing erbium oxide, Compos. Sci. Technol. 143 (2017) 67–74, https://doi.org/10.1016/j.compscitech.2017.03.002.
[24] B. Körpınar, B.C. Öztürk, N.F. Çam, H. Akat, Radiation shielding properties of Poly (hydroxylethyl methacrylate)/Tungsten(VI) oxide composites, Mater. Chem. Phys. 239 (2020) 121986, https://doi.org/10.1016/j.matchemphys.2019.121986.
[25] S.D. Kaloshkin, V.V. Tcherdyntsev, M.V. Gorshenkov, V.N. Gulbin, S.A. Kuznetsov, Radiation-protective polymer-matrix nanostructured composites, J. Alloys Compd. 536 (2012) S522–S526, https://doi.org/10.1016/j.jallcom.2012.01.061.
[26] V.I. Pavlenko, N.I. Cherkashina, Effect of SiO_2 crystal structure on the stability of polymer composites exposed to vacuum ultraviolet radiation, Acta Astronaut. 155 (2019) 1–9, https://doi.org/10.1016/j.actaastro.2018.11.017.
[27] N.I. Cherkashina, V.I. Pavlenko, A.V. Noskov, Radiation shielding properties of polyimide composite materials, Radiat. Phys. Chem. 159 (2019) 111–117, https://doi.org/10.1016/j.radphyschem.2019.02.041.
[28] R. Li, Y. Gu, Y. Wang, Z. Yang, M. Li, Z. Zhang, Effect of particle size on gamma radiation shielding property of gadolinium oxide dispersed epoxy resin matrix composite, Mater. Res. Express 4 (2017) 035035, , https://doi.org/10.1088/2053-1591/aa6651.
[29] I.M. Nikbin, M. Shad, G.A. Jafarzadeh, S. Dezhampanah, An experimental investigation on combined effects of nano-WO_3 and nano-Bi_2O_3 on the radiation shielding properties of magnetite concretes, Prog. Nucl. Energy 117 (2019) 103103, https://doi.org/10.1016/j.pnucene.2019.103103.
[30] V.I. Pavlenko, N.I. Cherkashina, R.N. Yastrebinsky, Synthesis and radiation shielding properties of polyimide/Bi_2O_3 composites, Heliyon 5 (2019) e01703, , https://doi.org/10.1016/j.heliyon.2019.e01703.
[31] A.M. El-Khatib, M.I. Abbas, M.A. Elzaher, M.S. Badawi, M.T. Alabsy, G.A. Alharshan, D.A. Aloraini, Gamma attenuation coefficients of nano cadmium oxide/high density polyethylene composites, Sci. Rep. 9 (2019) 16012, https://doi.org/10.1038/s41598-019-52220-7.
[32] F. El Haber, G. Froyer, Transparent polymers embedding nanoparticles for X-rays attenuation, J. Univ. Chem. Technol. Metall. 43 (2008) 283–290.
[33] V.N. Gulbin, V.F. Petrunin, Investigation of nanostructured radiation-protective composites, Phys. Procedia 72 (2015) 540–543, https://doi.org/10.1016/j.phpro.2015.09.048.
[34] A. Mesbahi, H. Ghiasi, Shielding properties of the ordinary concrete loaded with micro- and nano-particles against neutron and gamma radiations, Appl. Radiat. Isot. 136 (2018) 27–31, https://doi.org/10.1016/j.apradiso.2018.02.004.
[35] G.N. Akapiev, S.N. Dmitriev, B. Erler, V.V. Shirkova, A. Schulz, H. Pietsch, Ion track membranes providing heat pipe surfaces with capillary structures, Nucl. Instrum. Methods Phys. Res. Sect. B Beam Interact. Mater. Atoms 208 (2003) 133–136, https://doi.org/10.1016/S0168-583X(03)01182-0.
[36] V.V. Shirkova, S.P. Tretyakova, Physical and chemical basis for the manufacturing of fluoropolymer track membranes, Radiat. Meas. 28 (1997) 791–798, https://doi.org/10.1016/S1350-4487(97)00186-8.
[37] P. Wang, X. Wang, Y. Ling, M. Wang, S. Ding, W. Shen, Z. Wang, Y. Wang, F. Liu, Ultrafast selective ionic transport through heat-treated polyethylene terephthalate track membranes with sub-nanometer pores, Radiat. Meas. 119 (2018) 80–84, https://doi.org/10.1016/j.radmeas.2018.09.007.
[38] A. Danine, J. Schoenleber, J. Ghanbaja, F. Montaigne, C. Boulanger, N. Stein, Microstructure and thermoelectric properties of p-type bismuth antimony telluride nanowires synthetized by template electrodeposition in polycarbonate membranes, Electrochim. Acta 279 (2018) 258–268, https://doi.org/10.1016/j.electacta.2018.05.071.
[39] X.R. Zhu, C.M. Wang, Q.B. Fu, Z. Jiao, W.D. Wang, G.Y. Qin, J.M. Xue, Preparation of Ag/Cu Janus nanowires: electrodeposition in track-etched polymer templates, Nucl. Instrum. Methods Phys. Res. B: Beam Interactions Mater. Atoms 356 – 357 (2015) 57–61, https://doi.org/10.1016/j.nimb.2015.04.061.
[40] R. Gupta, R. Kumar, Influence of low energy ion beam implantation on Cu nanowires synthesized using scaffold-based electrodeposition, Nano-Struct. Nano-Objects 18 (2019) 100318, https://doi.org/10.1016/j.nanoso.2019.100318.
[41] D.L. Zagorskiy, V.V. Korotkov, K.V. Frolov, S.N. Sulyanov, V.N. Kudryavtsev, S.S. Kruglikov, S.A. Bedin, Track pore matrixes for the preparation of Co, Ni and Fe nanowires: electrodeposition and their properties, Phys. Procedia 80 (2015) 144–147, https://doi.org/10.1016/j.phpro.2015.11.090.
[42] M. Kac, A. Zarzycki, S. Kac, M. Kopec, M. Perzanowski, E.M. Dutkiewicz, K. Suchanek, A. Maximenko, M. Marszalek, Effect of the template-assisted electrodeposition parameters on the structure and magnetic properties of Conanowire arrays, Mat. Sci. Eng. B-SOLID 211 (2016) 75–84, https://doi.org/10.1016/j.mseb.2016.06.004.
[43] A. Dangwal, G. Müller, F. Maurer, J. Brötz, H. Fuess, Field emission properties of bare and gold-coated nickel nanowires grown in polymer ion-track membranes, J. Vac. Sci. Technol. B 25 (2007) 586, https://doi.org/10.1116/1.2709888.
[44] The file cabinet of Powder Diffraction Standards (PDS) card numbers in the form of Powder Diffraction File (PDF). http://www.icdd.com.
[45] A.A. Naberezhnov, A.E. Sovestnov, A.V. Fokin, Crystal structure of indium and lead under confined geometry conditions, Tech. Phys. 56 (2011) 637–641, https://doi.org/10.1134/S1063784211050240.
[46] W. Huda, R.M. Slone, Review of Radiologic Physics, LWW, third ed., (2009).
[47] D.L. Webster, P.A. Ross, The Compton effect, Nature 115 (1925) 51, https://doi.org/10.1038/115051a0.

Cherkashina N.I. was born in Belgorod, Russia in 1988. She received the Candidate of Engineering Sciences in condensed matter physics from the Belgorod State National Research University, Belgorod, Russia in 2013. Since 2013 she has been a Research Assistant with the Belgorod State Technological University named after V.G. Shoukhov (BSTU). Since 2013 she has been an associate Professor with the Radiation monitoring laboratory. Her research interest includes the radiation solid-state physics and space materials science. She is the author of two monographs, more than 100 articles, and 8 patents.

Pavlenko V.I. was born in Belgorod, Russia in 1949. He received the Candidate of Chemical Sciences in Physical chemistry from the Leningrad Institute of Technology, Saint Petersburg, Russia, in 1978 and the Doctor of Engineering Sciences in solid state physics from Moscow State University of Electronics and Mathematics, Moscow, Russia, in 1997. Since 2005 he has been a director of the Chemical Technology Institute, BSTU, Russia. His research interest includes the radiation solid-state physics and space materials science. He is the author of five books, more than 200 articles, and 18 patents. He is an Honored Inventor of the Russian Federation.

Noskov A.V. was born in Shevchenko, Kazakhstan in 1979. He received the Candidate of physical and mathematical sciences in Theoretical physics from the Belgorod State University, Belgorod, Russia, in 2004 and the Doctor of physical and mathematical sciences in Physics of the atomic nucleus and elementary particles from Skobeltsyn Research Institute of Nuclear Physics of Lomonosov Moscow State University, Moscow, Russia, in 2010. Since 2017 he has been a head of the Department of Theoretical and Mathematical Physics, BSU, Russia. He is the author of more than 100 articles.

Novosadov N.I. was born in Kurchatov, Kursk region, Russia in 1998. In 2016 he entered to study the Belgorod State Technological University named after V.G. Shoukhov (BSTU). Since 2019 he has been a Research Assistant with the Belgorod State Technological University named after V.G. Shoukhov (BSTU). His research interest includes the radiation solid-state physics and space materials science. He is the author of 5 articles.

Samoilova E.S. was born in Khabarovsk, Khabarovsk Territory, Russia in 1998. In 2016 she entered to study the Belgorod State Technological University named after V.G. Shoukhov (BSTU). Since 2019 he has been a Research Assistant with the Belgorod State Technological University named after V.G. Shoukhov (BSTU). Her research interest includes the radiation solid-state physics and space materials science. She is the author of 10 articles.